



OPEN

A study on improving the current density performances of CO₂ electrolyzers

Yueyuan Gu¹, Jucai Wei¹, Xu Wu¹✉ & Xiaoteng Liu²✉

Electrochemical CO₂ reduction reaction (CO₂RR) technology can reduce CO₂ emission with converting excess electrical energy to high-value-added chemicals, which however needs further improvement on the electrolyser cell performance. In this work, extensive factors were explored in continuous CO₂ electrolyzers. Gold, one of the benchmark materials for CO₂RR to produce CO, was used as the catalyst. Electrolyser configurations and membrane types have significant influences on cell performance. Compact MEA-constructed gas-phase electrolyser showed better catalytic performance and lower energy consumption. The gas diffusion electrode with a 7:1 mass ratio of total-catalyst-to-polytetrafluoroethylene (PTFE) ionomer exhibited the best performance. At a low total cell voltage of 2.2 V, the partial current density of CO production achieved 196.8 mA cm⁻², with 90.6% current efficiency and 60.4% energy efficiency for CO producing respectively. Higher CO selectivity can be achieved using anion exchange membranes, while higher selectivity for hydrogen and formate products can be achieved with cation exchange membranes. This research has pointed out a way on how to improve the CO₂RR catalytic performance in flow cells, leaving aside the characteristics of the catalyst itself.

Achieving the peak carbon dioxide emissions and carbon-neutral objective requires advanced CO₂ utilization technologies and reliable high-capacity renewable energy storage systems, for which the reduction of CO₂ to produce valuable chemicals by direct electrolysis is a promising approach^{1–5}. Currently, one of the main problems of CO₂ electrolyzers is the insufficient time–space yield or current density at working voltages^{6,7}.

In addition to the inherent properties of the cathode catalyst, all components of the flow-cell may have impacts on the electrolyser cell performance^{8,9}, including but not limited to electrode preparation processes^{10,11}, electrolyte compositions and concentrations, temperatures^{12,13}, gas pressures¹⁴, electrochemical membrane reactor configurations⁸, polymer electrolyte membranes¹⁵, and polymeric binders¹⁶. Jhong et al.¹⁰ compared the influence of catalyst layer deposition methodology on electrode catalytic performance, the partial current density of CO production (j_{CO}) obtained with the air-brushed cathode was higher (~87 mA cm⁻² at -1.68 V vs. Ag/AgCl) than that of the hand-painted cathode, with an increase of about 10 mA cm⁻². Kim et al.¹⁷ conducted a series of studies to explore the effects of the microporous layer (MPL) composition and the carbon paper substrate on CO₂RR performance. With a suitable MPL composition (20 wt% PTFE, 1 mg cm⁻² carbon), the j_{CO} achieved 280 mA cm⁻² at -2.20 V vs. Ag/AgCl, which was ten times that of the gas diffusion electrode (GDE) without MPL. Concerning the impact of the carbon paper substrate thickness, a higher j_{CO} (171.5 mA cm⁻², at -2.05 V vs. Ag/AgCl) was obtained with a thinner substrate (190 μm)¹⁷. Also, Kim et al.¹⁷ found that carbon paper with a lower wet proof level (10%) can obtain a higher j_{CO} (224 mA cm⁻² at -2.05 V vs. Ag/AgCl). However, research by Park et al.¹⁸ showed that the superhydrophobic carbon paper performed best, and the j_{CO} achieved 19.25 mA cm⁻² at -1.3 V vs. RHE. Of note, the carbon paper characteristics, flow-cell configurations, and operating conditions used in the above two studies were different. There was no unified conclusion on the effect of substrate hydrophobicity on CO₂RR performance. Lee et al.¹⁶ found that the PTFE binder exhibited the highest current efficiency for CO production among the five kinds of polymeric binders, 94.7% at -0.7 V vs. RHE. The mass ratio of catalysts-to-binders used in CO₂RR-related researches varied from 4:1 to 30:1^{19,20}, and even no polymeric binders were added sometimes¹⁵. The amount of polymeric binder added still needs optimization. Beyond the catalyst, there is still much to be done on improving the CO₂RR performance.

¹School of Environmental Science and Engineering, Huazhong University of Science and Technology, Wuhan 430074, China. ²Department of Mechanical and Construction Engineering, Faculty of Engineering and Environment, Northumbria University, Newcastle upon Tyne NE1 8ST, UK. ✉email: profxuwu@hust.edu.cn; terence.liu@northumbria.ac.uk

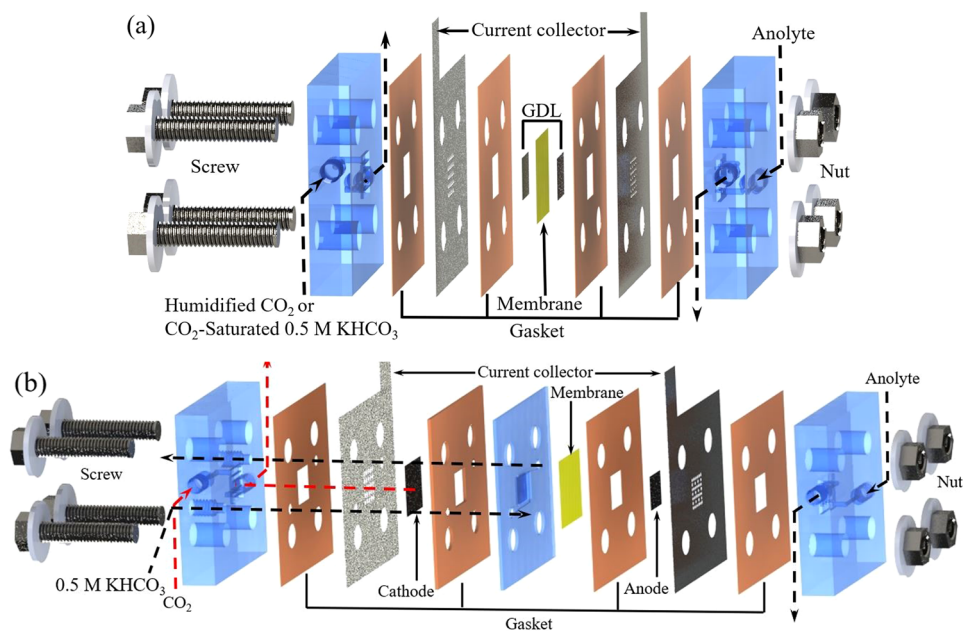


Figure 1. Expanded view of the CO₂ electrolyser: (a) zero-gap MEA configuration, (b) with a liquid buffer layer at the cathode side.

In this paper, extensive attempts have been made to obtain larger current density at lower cell potentials. First, two electrolyser structures and two different cathode feeding methods were tested and compared. The zero-gap MEA structure with low resistance was preferred, and the humidified gas-phase CO₂ was directly fed into the cathode to alleviate the mass transfer limitation caused by the low solubility of carbon dioxide in an aqueous solution. Then, through the test and comparison of Nafion and PTFE binders, it was found that adding a small amount of PTFE can improve the hydrophobicity of GDE and obtain a higher selectivity in CO production. Besides, the ion transfer mechanism of the anion exchange membrane was more advantageous in terms of catalytic reduction of CO₂ to CO.

Results and discussion

Influence of the electrolyser structures and the cathode feeding method. CO₂ electrolyser with two different structures were adopted in this paper, as shown in Fig. 1. Both adopted a common membrane electrode assembly (MEA) configuration^{7,21}, except that a liquid buffer layer was added at the cathode side of the second one. Two different cathode feeding methods were used in the MEA configuration (Fig. 1a). For the second one (Fig. 1b), there was a 2 mm thick liquid buffer layer between the membrane and cathode, CO₂ gas (dry) diffused from the back of the gas diffusion electrode to the catalyst surface.

The cell performances of the CO₂ electrolyser under three different conditions (Figure S3) were shown in Fig. 2. As shown in Fig. 2a, the total current densities obtained with humidified-CO₂ and liquid buffer layer were almost linearly related to the cell potential (resistance polarization control), and the resistances were 5.6 Ω and 16.6 Ω respectively. The total current density (j_{total}) obtained with CO₂-saturated KHCO₃ increased rapidly when the cell potential was higher than 2.2 V, obtained the highest value of 340.9 mA cm⁻² at 2.6 V. Combined with the product detection results (Fig. 2b), the current increase in this case mainly came from the side reaction of hydrogen evolution. The main products were CO and H₂, and the current efficiency of H₂ formation was not indicated in Fig. 2b.

The different cathode feeding methods affected the available CO₂ concentration on the catalyst surface. As shown in Fig. 2b, when the amount of available reactant gas CO₂ was sufficient (humidified-CO₂ feeding method), a current density for CO production (COCE) more than 80% was obtained between 1.8 V and 2.4 V, and the COCE gradually decreased from 2.2 V. Due to the low solubility of carbon dioxide in aqueous solution, there were not that much reactant gases used to produce CO with the CO₂-saturated KHCO₃ feeding method. Therefore, the total reduction current density obtained between 1.6 and 2.2 V was much lower than that of the gas-phase feeding method. Until the cell voltage was up to 2.4 V and 2.6 V, the H₂ evolution selectivity increased, and the total current density increased rapidly. The j_{CO} was in this order (see Fig. 2c): humidified-CO₂ > with diffusion layer > CO₂-saturated KHCO₃. The corresponding j_{CO} were 128.4 mA cm⁻², 54.1 mA cm⁻² and 0.4 mA cm⁻² at 2.6 V cell potential, respectively.

By adding a thin liquid pH buffer layer, a triple-phase boundary can be formed. The gas-phase CO₂ molecules can be quickly diffused to the surface of the catalyst (compared with that in the liquid phase), in this way the CO₂RR catalytic selectivity can be improved and the hydrogen evolution reaction can be partially suppressed²². According to Weekes et al.²³, the mass transfer limitations can be alleviated by using a gas-phase stream, thereby

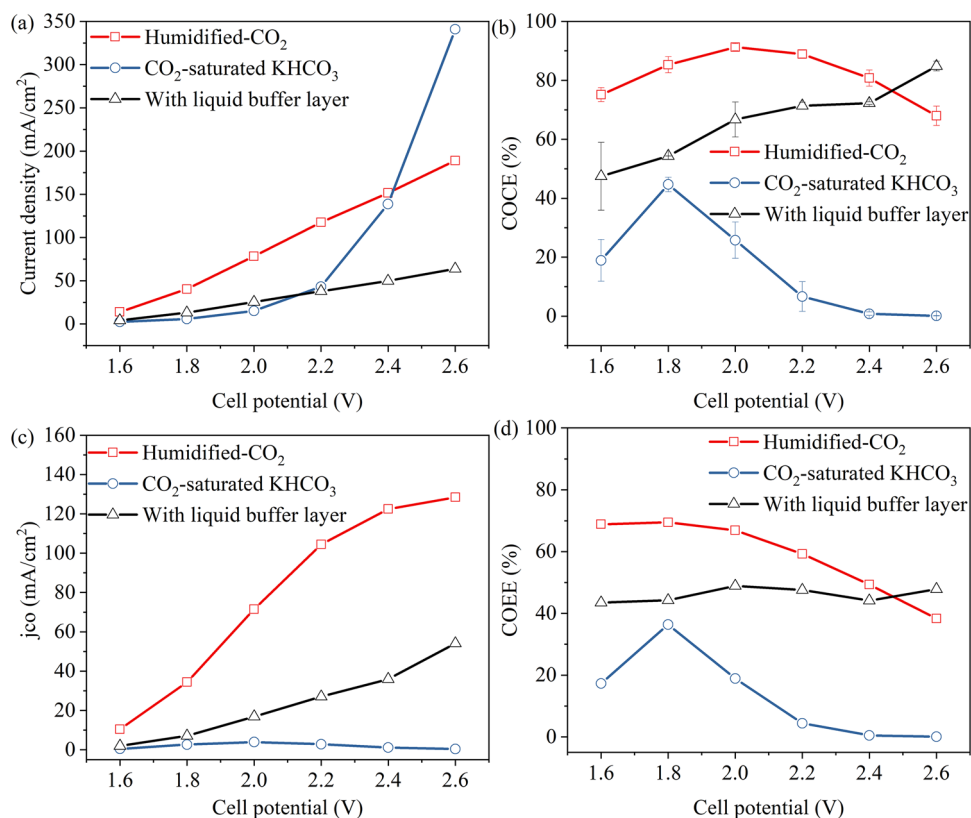


Figure 2. Cell performances acquired with different cathode feeding methods or electrolyser configurations. **(a)** Average total current density, **(b)** COCE, **(c)** average partial current density, and **(d)** COEE, as a function of the total cell potential.

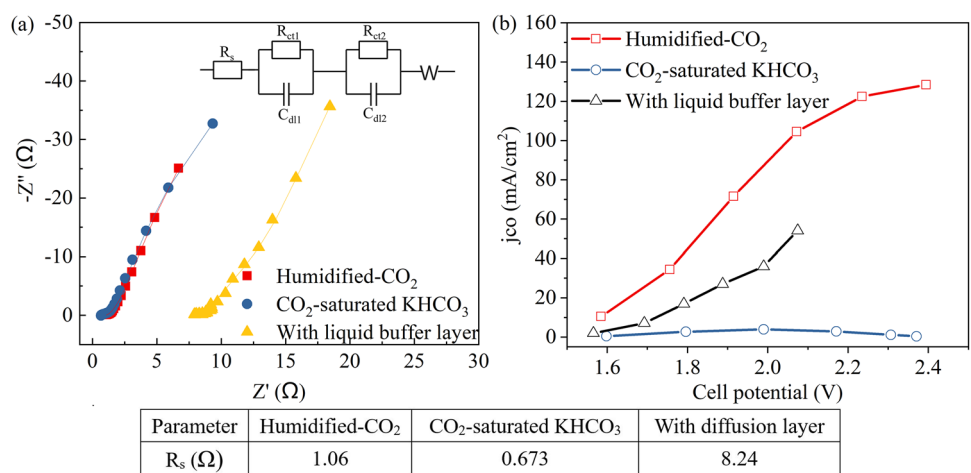


Figure 3. **(a)** EIS results and the relevant equivalent circuits acquired with different cathode feeding methods or configurations under open-circuit level. Points and lines represent measured and fitted results, respectively. **(b)** j_{CO} as a function of the cell potential (after iR compensation).

increasing the current density. This can explain why the j_{CO} obtained with CO₂-saturated KHCO₃ was the lowest (less than 4 mA cm⁻²), as the mass transfer of CO₂ molecules under this condition was the worst²⁴. When the cell potential was between 1.6 and 2.2 V, the energy efficiency for producing CO (COEE) obtained with humidified-CO₂ remained above 60% (see Fig. 2d).

As shown in Fig. 3a, the overall resistance between the two electrodes (R_s) increased significantly (from 1.06 to 8.24 Ω) after adding a liquid buffer layer. This explained the decrease in current density after adding a liquid

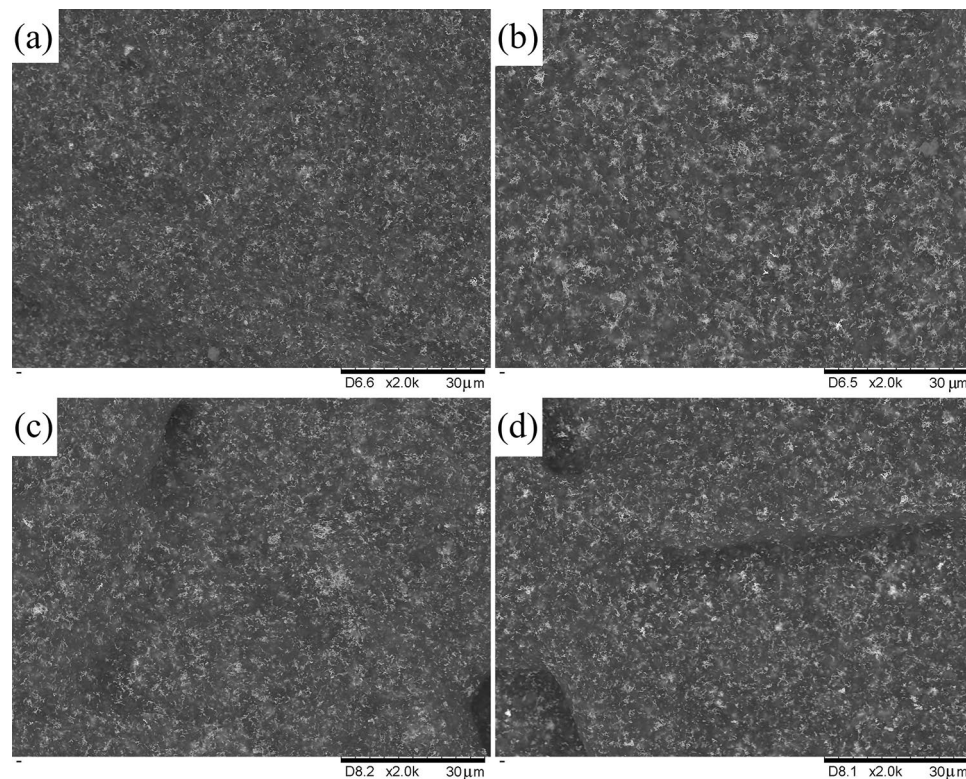


Figure 4. SEM images of top-down views of the gas diffusion electrodes with different Nafion ionomer additions (a) 3:1, (b) 5:1, (c) 7:1, (d) 10:1.

buffer layer, the large resistance led to the decrease of current density. This also means an increase in energy consumption in industrial applications. The Rs of the electrolyte feeding mode was smaller than that of the gas-phase mode. That is, under the same total cell voltage, the actual potential applied on the cathode with electrolyte feeding mode was slightly higher than that with gas-phase feeding mode, which also has some influence on the production selectivity. The thickness of the buffer layer needs to be extremely thin for better application⁸. As shown in Fig. 3b, after *iR* compensation, the best performance was still obtained with the MEA structure, humidified-CO₂ feeding method, so this mode was adopted in the following research.

Besides, a small number of hydrocarbons (CH₄, C₂H₄, and C₂H₆) were detected when using CO₂-saturated KHCO₃ as a catholyte. As shown in Figure S4, the current efficiency for CH₄ production was 2.3% at 2.4 V. In contrast, the CE of hydrocarbon product was negligible (less than 0.05%) in the tests under the other two conditions.

Binder types and contents. *Cell performance.* Two commonly used binders were used to prepare gas diffusion electrodes (GDE). The morphologies of GDE prepared with different Nafion contents were shown in Fig. 4. The catalyst layer was uniformly distributed on the surface of the gas diffusion electrode using the air-brush method. There was no obvious difference in the morphologies of the electrodes prepared with different Nafion contents.

As shown in Fig. 5a,c, j_{total} and j_{CO} were both in this order: 10:1 > 7:1 > 5:1 > 3:1. That is, the more Nafion binder added, the lower the current density. There was no obvious difference between the four samples in Fig. 5b except for the much lower COCEs of the 3:1 sample at high cell potentials (2.4 V and 2.6 V). The range of the four binder ratios was narrow, and the inherent properties of the Au/CN catalyst had a greater impact on catalytic performance, the COCE of the four samples followed the same trend. The j_{CO} of the 3:1 sample (the highest amount of Nafion added) was much lower than the other three samples, especially at 2.6 V, the j_{CO} was only 165.7 mA cm⁻², while the 10:1 sample was 259.5 mA cm⁻² (with 93.8 mA cm⁻² difference). This may be ascribed that Nafion is a hydrophilic resin with no hydrophobic gas-phase channels. Especially in high current density zones, adding too much Nafion may make it difficult for the reaction gas CO₂ to be transported to the catalyst surface²⁵. The COEE results were shown in Fig. 5d, and the highest energy efficiency (approximately 70%) was achieved at 1.8 V. When the mass ratio of total-catalyst-to-Nafion was 7:1, the j_{CO} reached 116.0 mA cm⁻² at 2.0 V cell potential, the COCE and COEE were 90.6% and 66.4%, respectively.

Similarly, four GDEs with different PTFE binder contents were prepared. The morphologies of GDEs were shown in Figure S5, and there was no obvious difference in appearance. As shown in Fig. 6a, there was not much difference in the total current density of the four electrodes, the total current density of the 3:1 sample was the lowest, similar to the results obtained with the Nafion binder. As the cell potential increased, the COCE of the four electrodes increased first and then decreased, reaching a maximum value (~90%) at 2.0 V (see Fig. 6b).

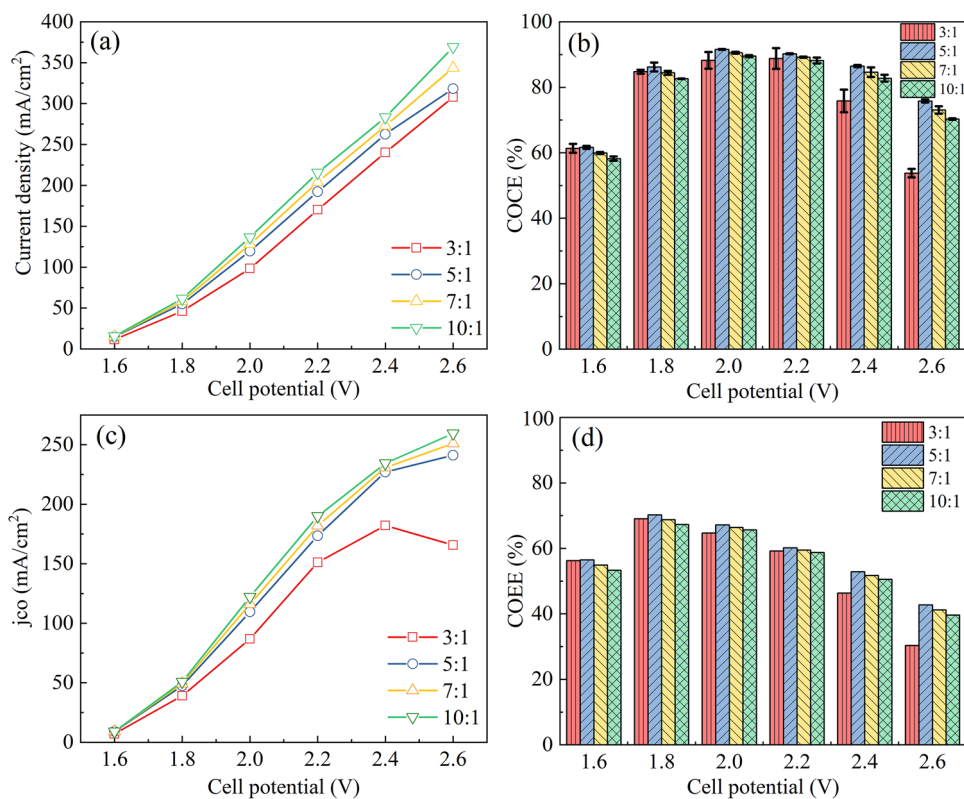


Figure 5. Cell performance of the electrodes with different Nafion contents. (a) j_{total} and (c) j_{CO} , (b) COCE and (d) COEE, as a function of the cell potential.

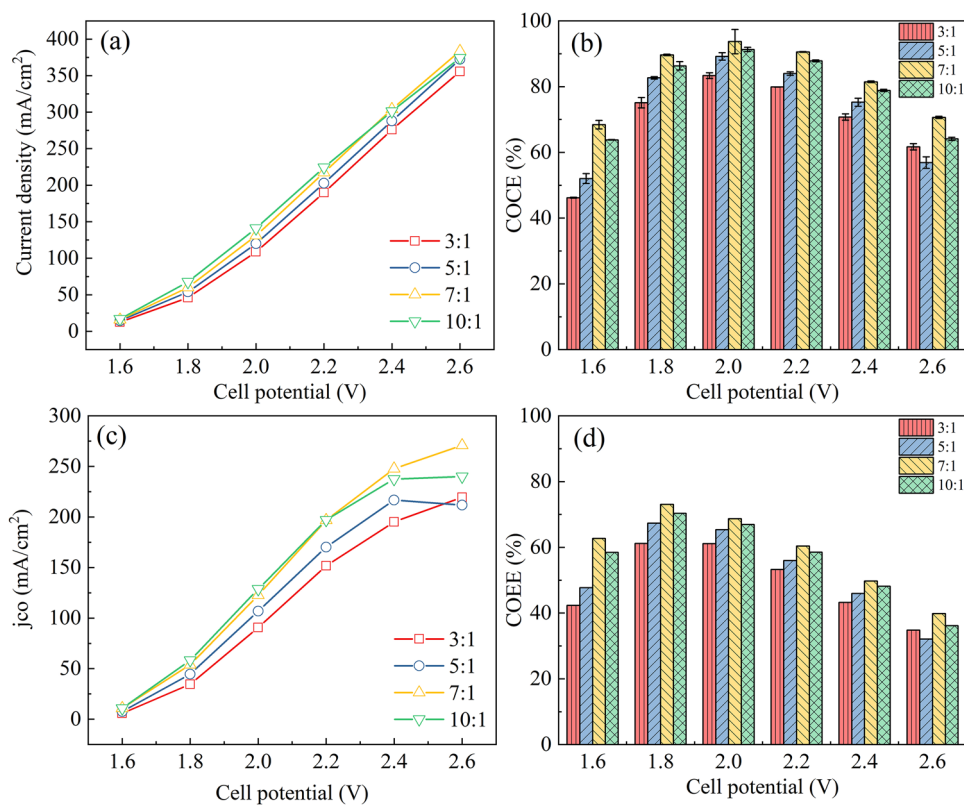


Figure 6. Cell performance of the electrodes with different PTFE contents. (a) j_{total} and (c) j_{CO} , (b) COCE and (d) COEE, as a function of the cell potential.

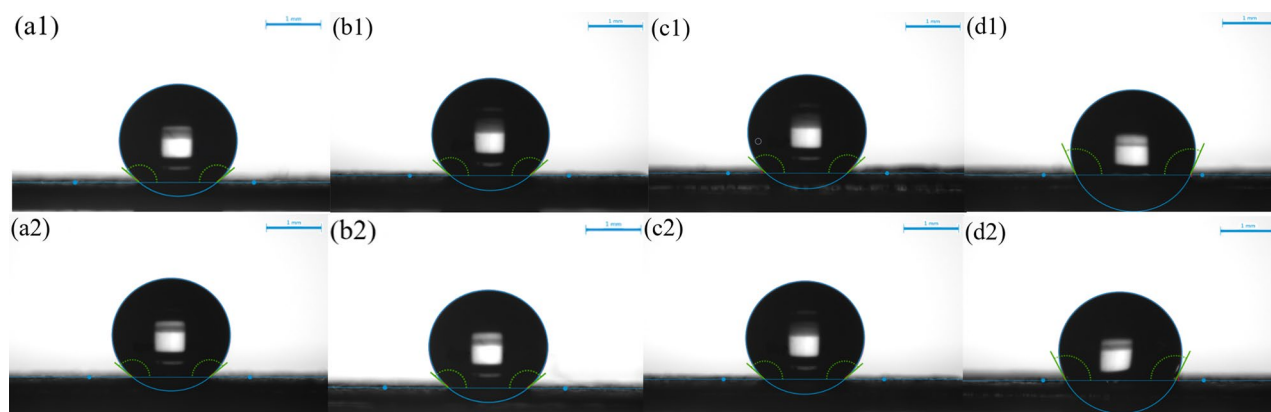
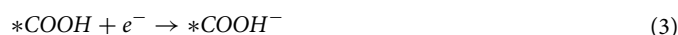
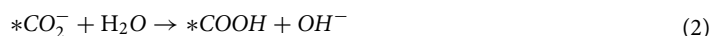


Figure 7. The contact angles of the air-brushed electrodes with different ionomer contents, (1) Nafion and (2) PTFE respectively. (a) 3:1, (b) 5:1, (c) 7:1, (d) 10:1.

Increasing the PTFE addition amount, the COCE of the four electrodes increased first and then decreased, reaching the maximum value when the mass ratio of total-catalyst-to-PTFE was 7:1. Except that at 2.6 V, the COCE of the 3:1 sample was slightly higher than that of 5:1. When the cell voltage was between 1.6 and 2.4 V, the j_{CO} of the 3:1 sample was lower than that of the 5:1 sample, but at 2.6 V, the j_{CO} of the 3:1 sample was higher than that of 5:1 (see Fig. 6c). The j_{CO} of the 7:1 sample reached 122.7 mA cm^{-2} at 2.0 V cell potential, with 93.7% COCE and 68.7% COEE. As shown in Fig. 6d, the maximum energy efficiency ($\sim 70\%$) was reached at 1.8 V, which was consistent with the results obtained with Nafion ionomer (see Fig. 5d).

Electrochemical and hydrophilicity characterization. Too much polymeric binder addition may have a cladding effect on gold particles, which will reduce the active surface area of the gold catalyst. If an Au particle is completely covered by an ionomer, or a C particle loaded with Au particles is covered by an ionomer, it is difficult to conduct electrons with the surrounding C particles. Under such conditions, these Au particles cannot conduct electrochemical reactions, and their surface areas cannot be measured by the CV curves²⁶. As shown in Figure S8, the CVs of the electrodes prepared with different binder contents coincide, and the calculated active surface area of gold was about 3.6 cm^2 (see Table S1). The slight differences in electrochemical surface area (ECSA) may come from weighing errors or pipetting errors. The addition ratios in this research did not have a coating effect on the surface of the gold particles or they are at the same cladding level. 20% to 35% of Nafion polymeric binder addition was generally considered suitable in water electrolyzers and fuel cells^{27,28}. The highest ratio (3:1) used in this study was included in this optimal range. Therefore, it can be considered that none of these four binder ratios hindered the utilization of gold catalysts.

The Tafel plots were shown in Figure S9, the corresponding Tafel slope and exchange current density (i_0) were shown in Table S1. For the Nafion binder, the Tafel slope of the 3:1 sample was significantly higher than the others, while the Tafel slope of the 7:1 sample was the minimum. For PTFE ionomer, the Tafel slope was in this order with a slightly difference: $10:1 < 7:1 < 5:1 < 3:1$. The lower Tafel slope indicates a faster first-electron transfer step²⁹, while higher i_0 indicates easier electrode polarization³⁰. The electrochemical reduction of CO_2 to CO on gold under neutral to alkaline pH can be written as follows^{31–33}, where * denotes an adsorption site:



If Eqs. (1) or (3) was the rate-determining step, the Tafel slope should be 116 and 39 mV dec^{-1} , respectively³⁴. The Tafel slope for all electrodes was between 143 to 187 mV dec^{-1} , the rate-determining step was closer to Eq. (1).

The static contact angles of water on the gas diffusion electrodes were shown in Fig. 7, and the corresponding specific angle values were shown in Table S1. For both Nafion and PTFE binders, the hydrophobicity of the electrode decreased as the binder content increased. GDEs prepared with PTFE binder were more hydrophobic than those prepared with Nafion binder. The water and gas distribution management of the GDE is important, and it needs to have the functions of gas transporting, liquid discharging, and electrons transferring³⁵. Moderate hydrophobicity can improve the management of gas and liquid distribution and decrease the possibility of electrode flooding. Nafion can conduct protons but not electrons, and the increased local proton concentration may promote hydrogen evolution reaction. PTFE can neither conduct electrons nor protons, but it can form

The mass ratio of catalyst and binder	j_{CO} (mA cm ⁻²)	Potential (V)	COCE (%)	COEE (%)	Mass activity for CO (A/g _{Au})	Temperature (°C)	Ref
7:1	122.7	2.0	93.8	68.7	613.5	RT	This work
7:1	196.8	2.2	90.6	60.4	984.1	RT	This work
7:1	247.7	2.4	81.5	49.8	1238.5	RT	This work
3:1	~ 148	3.0	88	43	1057	RT	7
Not given	> 425	3.0	> 85	> 42	> 1063	60	13
8:1	203	2.5	64	38	1128	RT	34
30:1	160	- 1.78 V vs. Ag/AgCl	> 60	-	941	RT	36
Not given	~ 4	2.0	62	45	231	RT	37
None	~ 28	- 1.3 V vs. RHE	77	-	-	RT	18

Table 1. Summary of reported CO₂ electrolyzers using Au catalyst.

hydrophobic pores, which is beneficial to water and gas distribution management¹⁶. However, adding a large amount of PTFE will increase the internal resistance of the electrode. There should be an optimum value in the balance between conductivity and hydrophobicity. In this study, the best performance was obtained with the 7:1 mass ratio of total-catalyst-to-PTFE.

As shown in Table 1, the CO₂ electrolyzers in this research exhibited excellent cell performance. RT means room temperature, and if no reference electrode was specified, then the potential signified total cell voltage. The mass ratio of catalyst and binder was estimated by the given parameters in each research. In this work, higher partial current density, current efficiency, and energy efficiency in producing CO can be obtained at a lower cell potential, and no heating source was required. The partial current densities for CO production obtained at 2.0 V, 2.2 V and 2.4 V were 122.7 mA cm⁻², 196.8 mA cm⁻² and 247.7 mA cm⁻², respectively. With such a low total cell potential of 2.2 V, a high mass activity for CO production of 985 A/g_{Au} was achieved at room temperature.

The influences of membranes. The CO₂RR performances with different membranes were shown in Fig. 8, the j_{total} values were in this order: G60 > FAA50 > N115 > PK75 (see Fig. 8a). The polarization curves of FAA50 and G60 membrane conform to ohmic polarization, and the calculated resistances are 5.6 Ω and 2.8 Ω, respectively. As shown in Fig. 8b,c, the N115 membrane exhibited the poorest catalytic performance on converting CO₂ to CO. Between 1.6 and 2.6 V, the COCE and the j_{CO} obtained with the N115 membrane was less than 40% and 10 mA cm⁻², respectively. And the COEE obtained with the N115 membrane was the lowest among the four membranes (see Fig. 8d). This phenomenon was consistent with Kutz et al.¹⁵, that the anion exchange membrane (AEM) exhibited better catalytic performance in the conversion of CO₂ to CO. With the use of AEM, the H⁺ will not be transported to the cathode, so the hydrogen evolution reaction was suppressed⁹. Among the three AEMs, the G60 membrane exhibited excellent catalytic performance. Under the same cell potential (from 1.8 to 2.6 V), the total current density obtained with the G60 membrane was almost twice that of the FAA50 membrane. Using the G60 membrane, the j_{CO} achieved 149.6 mA cm⁻² at 2.0 V, with high current efficiency (95.0%) and energy efficiency (69.7%) in the conversion of CO₂ to CO. This result was not surprising as the G60 membrane was developed especially for CO₂ electrolysis¹⁵, and has been commercialized and adopted by more and more researchers^{38–40}.

Combined with the EIS results in Figure S10, the total current density obtained with a smaller Rs was increased, which was the same as the previous test results under different configurations. According to the corresponding technical datasheet, the area resistance of the PK75 membrane (1.2–2.0 Ω cm⁻² in Cl⁻ form) is larger than that of the FAA50 membrane (0.6–1.5 Ω cm⁻² in Cl⁻ form), and the FAA50 membrane (45–55 μm) is thinner than the PK75 membrane (70–80 μm). This may explain why the Rs measured with the two membranes were nearly four times different. The best-performance G60 membrane is not only thin (50 μm) but also has the lowest average area resistance (0.045 Ω cm⁻²) under alkaline conditions.

Besides, hydrogen evolution reaction was more likely to occur when using N115 membrane, and so did the formate product. As shown in Figure S13 and S14, the current efficiency of formate obtained with N115 membrane was 23.6% at 2.2 V. No formate accumulation was observed when using anion exchange membranes. As shown in Figure S15, the formate concentration decreased with sample collection and deionized water replenishment.

Discussion

In this work, beyond the properties of the catalyst, we extensively explored the influence of many other factors on the selectivity of CO production in continuous CO₂ electrolyzers. Compared with the similar structure and operation mode of the H-cell, adding a thin liquid buffer layer between the cathode and the membrane can improve the catalytic performance by promoting the diffusion of CO₂ gas to the catalyst surface. A compact gas-phase MEA structure CO₂ electrolyser was preferred, which has lower Rs and excellent CO₂ gas mass transfer. PTFE was more suitable than Nafion as a binder for CO₂RR GDE preparation. When the mass ratio of total-catalyst-to-PTFE was 7:1, the total current density reached 131.0 mA cm⁻² at a low cell potential of 2.0 V, and the current efficiency and energy efficiency of CO production were 93.72% and 68.7%, respectively. Through the test

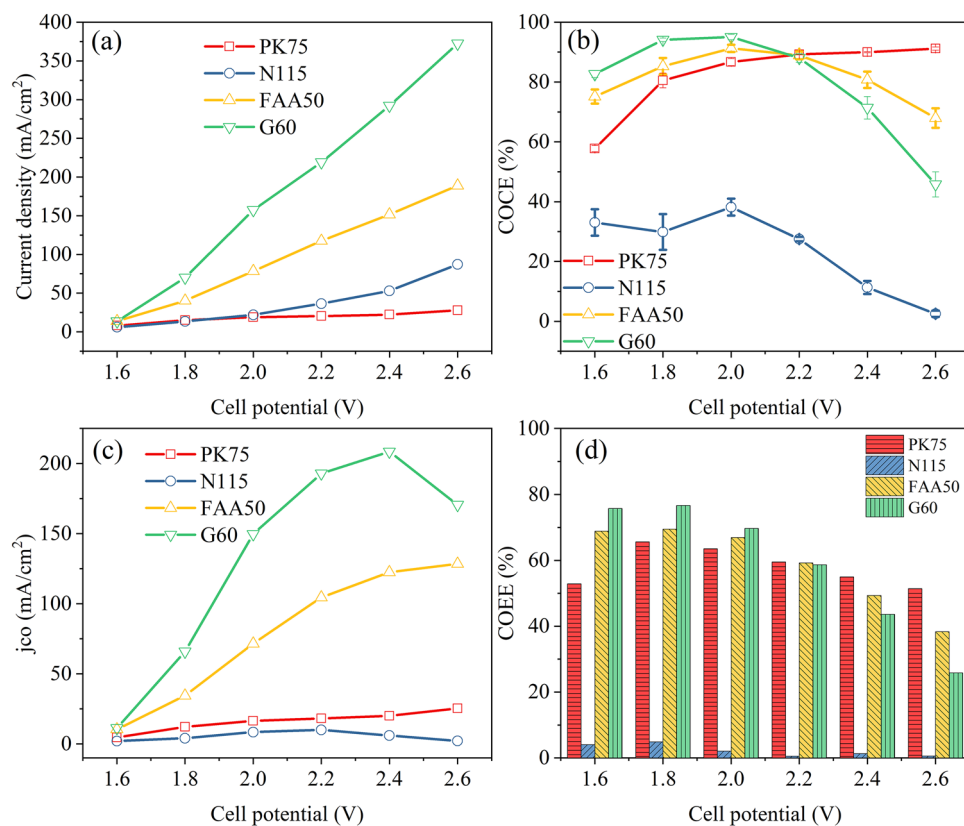


Figure 8. Cell performance acquired with different membrane. (a) j_{total} , (b) COCE, (c) j_{CO} , and (d) COSE, as a function of the cell potential.

and comparison of four kinds of membranes, it was found that the anion exchange membrane exhibited higher current efficiency and partial current density in the conversion of CO₂ to CO. Choosing the right membrane for different target products, then twice as much can be accomplished with half the effort. With the development of CO₂ electrolysis technology to continuous electrolyzers with high current density, our research may pave the way for other research groups to develop new catalysts in full-cell CO₂ electrolyzers. It is indeed of great interest to further study whether the conclusion obtained in this study is suitable for other kinds of catalysts.

Methods

Materials. KOH (≥85.0%), KHCO₃ (≥99.5%), urea (≥99.0%), NaBH₄ (≥98.0%), ethanol (≥99.7%), HClO₄ (70.0–72.0%), and HAuCl₄ (≥99.9%) was purchased from Shanghai Lingfeng and Shanghai Chemical Reagent Co., Ltd respectively; Nafion solution (5 wt%) and polytetrafluoroethylene dispersion (Teflon PTFE DISP 30LX) was purchased from Dupont; anion exchange membrane (Fumasep FAA-3-50), carbon black (Vulcan XC 72R) and carbon paper (Toray, TGP-H-60) was purchased via Fuel Cell Store website. All other chemicals were purchased from Sinopharm Chemical Reagent Co., Ltd. Milli-Q ultrapure water (Millipore, ≥18 MΩ·cm) was used throughout the work.

Characterizations. The morphologies and the phase identification of the Au/CN catalysts were examined by transmission electron microscopy (TEM, Hitachi HT7700) and X-ray diffraction (Haoyuan, DX-27mini) respectively. The X-ray photoelectron spectroscopy (Thermo ESCALAB 250XI) measurement was performed. The actual mass ratio of gold in the catalyst was determined by an inductively coupled plasma emission spectrometer (ICP, Optima8300DV). The morphologies of the spray-prepared cathode were analyzed by scanning electron microscopy (SEM, Hitachi TM3030). The hydrophobic and hydrophilic performance of the prepared electrodes were characterized by static contact angles (Dataphysics, JY-82B Krüss DSA100).

Catalysts and gas diffusion electrodes preparation. The Au nanoparticles supported on N-doped carbon (Au/CN) were synthesized by following our previous report⁷. The gold mass ratio of the Au/CN catalysts was 20 wt% and the particle size of gold nanoparticles was mainly distributed around 2 nm. Hydrophobic carbon paper (Toray, TGP-H-60) was used as the substrate, and no microporous layer was constructed. The Au/CN catalyst was dispersed in a solvent comprised of 1:1 (volume ratio) ethanol and water. After 20-min ultrasonication, 4 mg mL⁻¹ (calculated based on the total mass of catalyst) ink was obtained. For experiments on different cathode feeding methods and electrolyser structures, Nafion dispersion was used as the binder, the mass ratio of total-catalyst-to-binder was 3:1. To investigate the influence of binder on CO₂RR performance, dif-

ferent amounts of Nafion or PTFE dispersion (the mass ratios of total-catalyst-to-binder were 3:1, 5:1, 7:1, 10:1, respectively) were added. The total mass of catalyst loading of the gas diffusion electrode was $1.0 \pm 0.1 \text{ mg cm}^{-2}$. As-prepared electrodes need to be sintered for one hour before use, Nafion 130 °C and PTFE binders 330 °C, respectively. Nickel foam ($1 \times 1 \text{ cm}^2$) was used as an anode catalyst to facilitate oxygen evolution. For three-electrode tests, 6.3 μL ink was dropped on the glassy carbon electrode with a diameter of 4 mm and dried at room temperature, making a mass loading of 0.2 mg cm^{-2} (calculated based on the total mass of catalyst).

Full-cell tests. For the MEA structure, the humidified CO_2 or CO_2 -saturated 0.5 M KHCO_3 was induced into the cathode chamber, while 2 M KOH was circulated in the anode chamber. Under the three operation conditions (Figure S3), the flow rates of gas and liquid were set to 15 sccm and 30 ml min^{-1} , respectively. Four different polymer electrolyte membranes, Fumasep FAA-3-PK-75, Nafion 115, Fumasep FAA-3-50, and Sustainion X37-50 Grade 60 were used in this research. For ease of illustration, they are referred to as PK75, N115, FAA50, and G60, respectively. Except for the membrane-related tests, the Fumasep FAA-3-50 membrane was used in other tests.

At each given cell voltage (1.6 V, 1.8 V, 2.0 V, 2.2 V, 2.4 V, and 2.6 V), a 20-min electrolytic test was performed using an electrochemical workstation (IVIUM, CompactStat.h A32718). The export gas was passed into deionized water to absorb liquid phase product. The actual gas outlet flow rate was monitored by a mass flow meter (Sevenstar, D07), 1 mL of the dried effluent gas was sampled automatically into a gas chromatograph (GC-2030) every ten minutes. At the end of electrolysis under each given cell voltage, 3 mL water absorption liquid was extracted and 3 mL deionized water was replenished. Formate concentration was examined by UV spectrophotometer (Metash, UV-5800H). At least two fresh-made parallel electrodes were tested for each sample. The electrochemical impedance spectroscopy (EIS) measurements were conducted from 100 kHz to 1 Hz with 10 mV amplitude under open circuit potential. There was no reference electrode included in the flow cell and no iR compensation was made unless otherwise specified. All the experiments were carried out at room temperature (25 °C) and ambient pressure.

Electrochemical measurements. For the three-electrode system tests, a Pt foil and saturated calomel electrode (SCE) were used as the counter electrode and reference electrode respectively. Linear sweep voltammetry (LSV) scans were performed at 1 mV s^{-1} in 0.5 M KHCO_3 saturated with CO_2 (pH 7.3). The ECSA of the Au catalyst was calculated by the reduction peak area measured in 0.1 M HClO_4 . And $390 \mu\text{C cm}^{-2}$ was used as the reference charge value for Au^{41} .

The current efficiency (CE) of a specific product is defined by the ratio of charge consumed in forming the product to the total charge consumed. The energy efficiency (EE) is defined by the ratio between the thermodynamic voltage to the practical cell voltage. The energy efficiency of CO (COCE) needs to be multiplied by its current efficiency⁷.

Received: 13 March 2021; Accepted: 4 May 2021

Published online: 27 May 2021

References

- Bailera, M., Lisbona, P., Romeo, L. M. & Espatolero, S. Power to Gas projects review: Lab, pilot and demo plants for storing renewable energy and CO_2 . *Renew. Sust. Energ. Rev.* **69**, 292–312 (2017).
- Gahleitner, G. Hydrogen from renewable electricity: An international review of power-to-gas pilot plants for stationary applications. *Int. J. Hydrog. Energy*. **38**, 2039–2061 (2013).
- Lehner, M., Tichler, R., Steinmuller, H. & Koppe, M. In *Power-to-Gas: Technology and Business Models*. 1–93 (SpringerBriefs in Energy, 2014).
- Fan, L.-S., Zeng, L., Wang, W. & Luo, S. Chemical looping processes for CO_2 capture and carbonaceous fuel conversion—Prospect and opportunity. *Energy Environ. Sci.* **5**, 7254–7280 (2012).
- Lu, Q. & Jiao, F. Electrochemical CO_2 reduction: Electrocatalyst, reaction mechanism, and process engineering. *Nano Energy* **29**, 439–456 (2016).
- de Arquer, F. P. G. *et al.* CO_2 electrolysis to multicarbon products at activities greater than 1 A cm^{-2} . *Science* **367**, 661–666 (2020).
- Gu, Y., Wei, J., Li, J., Wang, L. & Wu, X. Long-term-stable continuous flow CO_2 reduction electrolyzers with high current efficiency. *Sustain. Energy Fuels*. **5**, 758–766 (2021).
- Vennekoetter, J.-B., Sengpiel, R. & Wessling, M. Beyond the catalyst: How electrode and reactor design determine the product spectrum during electrochemical CO_2 reduction. *Chem. Eng. J.* **364**, 89–101 (2019).
- Gu, Y., Wei, J., Li, J., Wang, L. & Wu, X. Overview and prospect of studies on electrochemical reduction of carbon dioxide electrolyzers. *Energy Storage Sci. Technol.* **9**, 1691–1701 (2020).
- Jhong, H.-R.M., Brushett, F. R. & Kenis, P. J. A. The effects of catalyst layer deposition methodology on electrode performance. *Adv. Energy Mater.* **3**, 589–599 (2013).
- Dinh, C.-T., García de Arquer, F. P., Sinton, D. & Sargent, E. H. High rate, selective, and stable electroreduction of CO_2 to CO in basic and neutral media. *ACS Energy Lett.* **3**, 2835–2840 (2018).
- Sebastián, D. *et al.* CO_2 reduction to alcohols in a polymer electrolyte membrane co-electrolysis cell operating at low potentials. *Electrochim. Acta*. **241**, 28–40 (2017).
- Yin, Z. *et al.* An alkaline polymer electrolyte CO_2 electrolyzer operated with pure water. *Energy Environ. Sci.* **12**, 2455–2462 (2019).
- Ramdin, M. *et al.* High pressure electrochemical reduction of CO_2 to formic acid/formate: A comparison between bipolar membranes and cation exchange membranes. *Ind. Eng. Chem. Res.* **58**, 1834–1847 (2019).
- Kutz, R. B. *et al.* Sustainion imidazolium-functionalized polymers for carbon dioxide electrolysis. *Energy Technol.* **5**, 929–936 (2017).
- Lee, J. H. *et al.* Understanding the role of functional groups in polymeric binder for electrochemical carbon dioxide reduction on gold nanoparticles. *Adv. Funct. Mater.* **28**, 1804762 (2018).
- Kim, B., Hillman, F., Ariyoshi, M., Fujikawa, S. & Kenis, P. J. A. Effects of composition of the micro porous layer and the substrate on performance in the electrochemical reduction of CO_2 to CO. *J. Power Sources*. **312**, 192–198 (2016).

18. Park, G., Hong, S., Choi, M., Lee, S. & Lee, J. Au on highly hydrophobic carbon substrate for improved selective CO production from CO₂ in gas-phase electrolytic cell. *Catal. Today* **355**, 340–346 (2019).
19. Leonard, M. E., Clarke, L. E., Forner-Cuenca, A., Brown, S. M. & Brushett, F. R. Investigating electrode flooding in a flowing electrolyte, gas-fed carbon dioxide electrolyzer. *Chemsuschem* **13**, 400–411 (2020).
20. Ma, S. *et al.* One-step electrosynthesis of ethylene and ethanol from CO₂ in an alkaline electrolyzer. *J. Power Sources* **301**, 219–228 (2016).
21. Gu, Y. *et al.* Template-free Cu electrodeposition to prepare Cu-micro-brush electrodes for electrochemical CO₂ reduction. *ChemistrySelect* **4**, 10995–11001 (2019).
22. Ma, Y., Shi, R. & Zhang, T. Research progress on triphase interface electrocatalytic carbondioxide reduction. *Acta Chim. Sin.* 1–11.
23. Weekes, D. M., Salvatore, D. A., Reyes, A., Huang, A. & Berlinguette, C. P. Electrolytic CO₂ reduction in a flow cell. *Acc. Chem. Res.* **51**, 910–918 (2018).
24. Delacourt, C., Ridgway, P. L., Kerr, J. B. & Newman, J. Design of an electrochemical cell making syngas (CO+H₂) from CO₂ and H₂O reduction at room temperature. *J. Electrochem. Soc.* **155**, B42–B49 (2008).
25. Wilson, M. S. & Gottesfeld, S. Thin-film catalyst layers for polymer electrolyte fuel cell electrodes. *J. Appl. Electrochem.* **22**, 1–7 (1992).
26. Cheng, X., Yi, B., Zhang, J., Han, M. & Qiao, Y. Influence of PTFE and nafion on the utilization efficiency of Pt/C catalyst in PEMFC. *Electrochemistry* **02**, 3–5 (1999).
27. Cheng, X. *et al.* Investigation of platinum utilization and morphology in catalyst layer of polymer electrolyte fuel cells. *J. Power Sources* **79**, 75–81 (1999).
28. Xu, W. & Scott, K. The effects of ionomer content on PEM water electrolyser membrane electrode assembly performance. *Int. J. Hydrog. Energy* **35**, 12029–12037 (2010).
29. Liu, M. *et al.* Enhanced electrocatalytic CO₂ reduction via field-induced reagent concentration. *Nature* **537**, 382–386 (2016).
30. Brad, A. & Faulkner, L. *Electrochemical Methods: Fundamentals and Applications*. 1–864 (1980).
31. Hori, Y. Electrochemical CO₂ reduction on metal electrodes. In *Modern Aspects of Electrochemistry*. 89–189 (Springer, 2008).
32. Chen, L. D., Urushihara, M., Chan, K. & Norskov, J. K. Electric field effects in electrochemical CO₂ reduction. *Acc. Catal.* **6**, 7133–7139 (2016).
33. Ma, Z. *et al.* Enhancing CO₂ electroreduction with Au/pyridine/carbon nanotubes hybrid structures. *Chemsuschem* **12**, 1724–1731 (2019).
34. Verma, S. *et al.* Insights into the low overpotential electroreduction of CO₂ to CO on a supported gold catalyst in an alkaline flow electrolyzer. *Acc. Energy Lett.* **3**, 193–198 (2018).
35. Dinh, C.-T. *et al.* CO₂ electroreduction to ethylene via hydroxide-mediated copper catalysis at an abrupt interface. *Science* **360**, 783–787 (2018).
36. Jhong, H.-R.M. *et al.* Gold nanoparticles on polymer-wrapped carbon nanotubes: An efficient and selective catalyst for the electroreduction of CO₂. *ChemPhysChem* **18**, 3274–3279 (2017).
37. Chung, Y.-H. *et al.* Polyethylenimine-assisted synthesis of Au nanoparticles for efficient syngas production. *Electroanalysis* **31**, 1401–1408 (2019).
38. Yang, H., Kaczur, J. J., Sajjad, S. D. & Masel, R. I. Electrochemical conversion of CO₂ to formic acid utilizing Sustainion™ membranes. *J. CO₂ Util.* **20**, 208–217 (2017).
39. Pellerite, M. *et al.* Imidazolium-functionalized polymer membranes for fuel cells and electrolyzers. *ECS Trans.* **80**, 945–956 (2017).
40. Jiang, K. *et al.* Isolated Ni single atoms in graphene nanosheets for high-performance CO₂ reduction. *Energy Environ. Sci.* **11**, 893–903 (2018).
41. Jin, L. *et al.* Ultrasmall Au nanocatalysts supported on nitrated carbon for electrocatalytic CO₂ reduction: the role of the carbon support in high selectivity. *Nanoscale* **10**, 14678–14686 (2018).

Acknowledgements

The authors would like to acknowledge the Thousands Youth Talents Project of China, which sponsors Prof. Xu Wu.

Author contributions

Y.G. carried out the experiment and wrote the manuscript with support from J.W. X.W. and X.L. helped supervise the project and contributed to the final version of the manuscript. All authors discussed the results and contributed to the final manuscript.

Competing interests

The authors declare no competing interests.

Additional information

Supplementary Information The online version contains supplementary material available at <https://doi.org/10.1038/s41598-021-90581-0>.

Correspondence and requests for materials should be addressed to X.W. or X.L.

Reprints and permissions information is available at www.nature.com/reprints.

Publisher's note Springer Nature remains neutral with regard to jurisdictional claims in published maps and institutional affiliations.



Open Access This article is licensed under a Creative Commons Attribution 4.0 International License, which permits use, sharing, adaptation, distribution and reproduction in any medium or format, as long as you give appropriate credit to the original author(s) and the source, provide a link to the Creative Commons licence, and indicate if changes were made. The images or other third party material in this article are included in the article's Creative Commons licence, unless indicated otherwise in a credit line to the material. If material is not included in the article's Creative Commons licence and your intended use is not permitted by statutory regulation or exceeds the permitted use, you will need to obtain permission directly from the copyright holder. To view a copy of this licence, visit <http://creativecommons.org/licenses/by/4.0/>.

© The Author(s) 2021